The Astrophysical Journal, 644:378–384, 2006 June 10

POSTLAUNCH ANALYSIS OF *SWIFT*'S GAMMA-RAY BURST DETECTION SENSITIVITY

David L. Band[1,2]

Received 2005 December 21; accepted 2006 February 10

ABSTRACT

The dependence of *Swift*'s detection sensitivity on a burst's temporal and spectral properties shapes the detected burst population. Using simplified models of the detector hardware and the burst trigger system, I find that *Swift* is more sensitive to long, soft bursts than *CGRO*'s BATSE, a reference detector because of the large burst database it has accumulated. *Swift* has increased sensitivity in the parameter space region into which time dilation and spectral redshifting move high-redshift bursts.

Subject headings: gamma rays: bursts — instrumentation: detectors

1. INTRODUCTION

The gamma-ray bursts that *Swift* (Gehrels et al. 2004) detects depend on the physical properties of the Burst Alert Telescope (BAT), *Swift*'s gamma-ray detector, and on BAT's triggering system. The dependence of BAT's detection sensitivity on a burst's temporal and spectral characteristics shapes the burst population that *Swift* studies. While the *Swift* observations are revealing a wealth of new phenomena through the study of individual bursts, we also want to relate these bursts to the bursts studied by previous missions. In particular, because of the large and statistically well-defined sample of more than 2700 bursts it has collected, the Burst and Transient Source Experiment (BATSE) on the *Compton Gamma-Ray Observatory (CGRO)* is the reference detector to which subsequent detectors such as BAT are compared. Therefore, in this work I use BAT's on-orbit calibration to gain a deeper understanding of the detector's sensitivity to different types of bursts. The insight from this study will help the design of future missions, such as *EXIST* (Grindlay 2005).

BAT detects approximately 100 bursts per year. Compared to BATSE's burst sample, a higher fraction of the bursts BAT detects are long-duration ($T_{90} > 2$ s) bursts (see Fig. 1), although the few short-duration bursts that have been detected have been particularly revelatory. Understanding the observed duration distribution is a goal of this work.

Evaluating BAT's burst detection sensitivity requires understanding the sequence of events on board the spacecraft. Bursts are detected by BAT (Barthelmy et al. 2005), a large field of view (FOV 1.4 sr), 15–150 keV coded mask detector with a 5200 cm^2 cadmium-zinc-telluride (CZT) detector plane. BAT's detector plane is sensitive to higher energy photons, but burst imaging and spectroscopy have an effective high-energy cutoff of $\sim$150 keV. Once BAT detects a burst, the spacecraft slews autonomously (within operational constraints) to place the burst location in the center of the much smaller FOVs of the X-Ray Telescope (XRT; Burrows et al. 2005, Osborne et al. 2005) and the co-aligned UV-Optical Telescope (UVOT; Roming et al. 2005). Thus BAT's trigger system determines which bursts are detected, although the other two detectors' performance and operational constraints affect whether the afterglow is followed by *Swift* immediately after the burst.

BAT's flight software detects bursts on board in two steps (Fenimore et al. 2003, 2004; Palmer et al. 2004). A rate trigger monitors the count rate from the CZT detectors for a statistically significant increase; BAT's rate trigger is complex, testing the count rate from the detector plane (and subsections of the plane) on timescales ranging from 0.004 to 32 s using a variety of different background estimates. Once a rate trigger occurs, an image is formed through the coded mask system. To maximize the signal-to-noise ratio (S/N) of the counts used for imaging, the software varies the energy band and the "foreground" time period over which the counts are accumulated. The software also uses different "background" time periods before, and perhaps after, the foreground time period from which the background during the foreground period is estimated. A number of images may be formed using different foreground time periods before the significance exceeds a detection threshold or the software concludes that a detection is not possible. Only if a new statistically significant point source is evident in an image is a burst considered to be detected. Periodically (once every 64 and 320 s, and when the spacecraft changes its orientation; Palmer et al. 2004; McLean et al. 2004) an image is formed and checked for a new point source even without a rate trigger. Because a burst detection requires the imaging of a new point source, the threshold for the rate trigger is set to permit many false positives that are subsequently rejected by the imaging step. Consequently, the imaging step is usually the most restrictive step and therefore determines BAT's burst sensitivity.

BAT's trigger system is complex, with many triggers and background estimates (Fenimore et al. 2003, 2004; Palmer et al. 2004). The flight software turns triggers on and off based on the computational load. While diagnostics are telemetered to the ground, the telemetry stream cannot provide sufficient data to reproduce on the ground the behavior of the trigger system precisely at all times. The complexity of the trigger system maximizes BAT's sensitivity—*Swift*'s design goal—at the expense of making an accurate determination of this sensitivity at a given time very difficult if not impossible. In particular, BAT achieves high image sensitivity by accumulating counts over much longer timescales than BATSE did, making the trigger sensitive to the details of the burst light curve. In contrast to burst spectra whose shapes are adequately described by two or three parameters, light curves differ greatly from burst to burst when considered on timescales greater than 1 s, and cannot be parameterized for sensitivity calculations by only a few parameters.

Despite all these caveats, I develop a semiquantitative understanding of the burst populations that BAT detects using a simplified model of BAT's trigger system that captures the essential features of the trigger. I assume that imaging is the most restrictive step of the trigger, and therefore ignore the complexity

[1] Code 661, NASA Goddard Space Flight Center, Greenbelt, MD 20771.
[2] Joint Center for Astrophysics, Physics Department, University of Maryland, Baltimore County, 1000 Hilltop Circle, Baltimore, MD 21250.

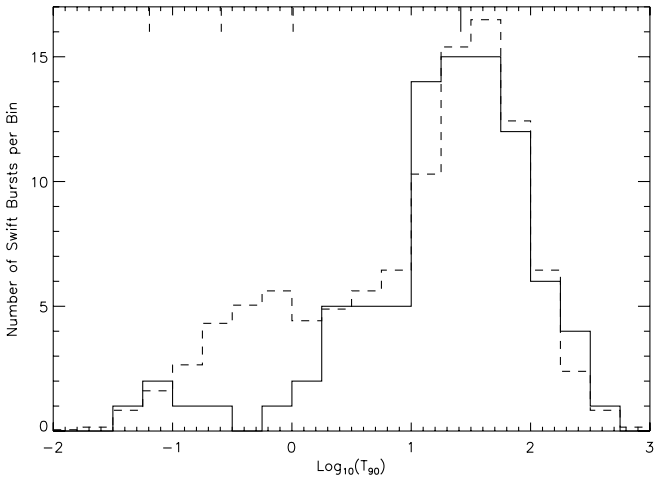

FIG. 1.—T_{90} distribution for *Swift* (*solid histogram*) and BATSE (*dashed histogram*). An arbitrary normalization was used for the 2041 BATSE bursts. *Swift* detects few of the short-duration bursts that BATSE detected. The *Swift* distribution includes bursts up to mid December 2005. The three short vertical dashed lines at the top of the plot indicate the Δt values used by the BATSE trigger, while the solid line indicates the maximum Δt value used by the BAT trigger system (the minimum value is less than the smallest T_{90} plotted).

of the rate trigger. I use a S/N estimate of the sensitivity of the imaging step. This calculation captures the fundamental dependence of BAT's sensitivity on a burst's hardness and duration. Calculations with greater verisimilitude would result from applying BAT trigger code to simulated burst data; the BAT team maintains a working copy of the trigger code incorporated in the flight software. Before launch such simulations were run to verify the performance of BAT and its flight software (Fenimore et al. 2004) and to determine the trigger system's initial settings (McLean et al. 2004). The simulated bursts should be accurate representations of the bursts BAT might detect.

I separate my evaluation of burst sensitivity into the dependencies on the burst's spectrum and light curve. This is an approximation, since a burst's spectrum changes during the burst (usually the spectrum softens with time; Ford et al. 1995), and the light curve depends on the energy band (usually individual pulses and the duration of the entire burst are shorter at high energy). After first providing the formulae for the detection significance for rate and image triggers (§ 2.1), I evaluate BAT's energy-dependent (§ 2.2) and duration-dependent (§ 2.3) burst sensitivity. I use these results to understand the observed burst population (§ 3). While I have discussed the factors affecting BAT's sensitivity with the members of BAT instrument team, the conclusions are my own. I use preliminary values for the performance of the instrument and the mission, and thus my sensitivities calculated using a simple model of the BAT trigger should be regarded as illustrative, not definitive.

2. BAT BURST SENSITIVITY

2.1. *Burst Triggers*

While they involve very different operations, rate and imaging triggers both analyze the counts accumulated by a burst detector over an energy band ΔE and accumulation time Δt; BAT's flight software analyzes overlapping energy bands (see § 2.2) and accumulation times (see § 2.3). For BAT, the initial rate trigger and the image with a statistically significant point-source detection need not use the same ΔE and Δt. If a burst is present, then the number of observed counts in ΔE and Δt is the sum of the counts from the burst C_s and the background B.

Rate and imaging triggers have similar dependencies on source and background counts, and thus analogous methods can be used to evaluate the resulting sensitivities. Before *HETE-II* and BAT, most burst detectors, such as BATSE, used

$$S_r = C_s/\sqrt{B} \tag{1}$$

as the detection significance for a rate trigger: the increase in the number of counts over the background is compared to the background's fluctuation scale. For a trigger, S_r must exceed a threshold value. To mitigate difficulties that occur when B is very large or very small, BAT's rate trigger replaces the background B in the denominator of equation (1) with a sum D of terms (see eq. [3] of Fenimore et al. 2003). When B is small, D asymptotes to a constant, while D asymptotes to B^2 when B is large, converting the detection criterion from a signal-to-noise to a signal-to-background ratio. For intermediate values of B, D is approximately equal to B.

The significance of a point source in a coded mask image is (G. Skinner 2005, private communication)

$$S_i = \frac{f_m C_s}{\sqrt{C_s + B}}, \tag{2}$$

where the factor f_m compensates for the finite size of the detector pixels relative to the mask elements. One interpretation of this factor of f_m is that the finite size of the detector pixels smears images on the sky, thereby lowering their significance. G. Skinner (2005, private communication) finds $f_m = 0.73$ for BAT, which explains why the rate trigger significance is greater than the image significance for the bursts BAT detects (D. Palmer 2005, private communication). The fluctuation level for an image includes the source counts in addition to the background counts (i.e., the denominator in eq. [2] is $(C_s + B)^{1/2}$ and not $B^{1/2}$) because the burst counts are merely background for positions on the sky other than that of the burst (the origin of C_s).

The rate trigger significance S_r in equation (1) is applicable to BATSE but not to BAT's rate trigger, for which the significance differs significantly from S_r in equation (1) for both small and large numbers of background counts. However, imaging is almost always the most restrictive step in BAT's burst detection algorithm, and therefore I only consider the sensitivity resulting from imaging. In comparing BATSE and BAT sensitivities, I use equation (1) for BATSE and equation (2) for BAT. I also assume that the BAT flight software successfully finds the "foreground" time period (the time period used for imaging) that maximizes the S/N, thereby optimizing the image step.

In the analysis that follows I first consider the energy dependence of S_i holding the accumulation time Δt fixed at 1.024 s (§ 2.2), a background-dominated case that allows me to use the methodology developed for rate triggers (Band 2003). Subsequently I consider the dependence on burst duration (§ 2.3).

2.2. *Energy Dependence*

In this subsection I assume that $\Delta t = 1.024$ s, for which the background dominates the burst counts at threshold (i.e., $B \gg C_s$). I calculate the number of source counts C_s by convolving the burst spectrum with the effective area over the energy band ΔE. Figure 2 shows the current understanding of BAT's detector efficiency (D. Hullinger 2005, private communication), here defined as the effective area on-axis divided by *half* of the area of the detector plane (the detector plane area is divided by 2 to account for the coded mask); thus, this efficiency is equivalent to the efficiency for a detector with half the area and no mask.

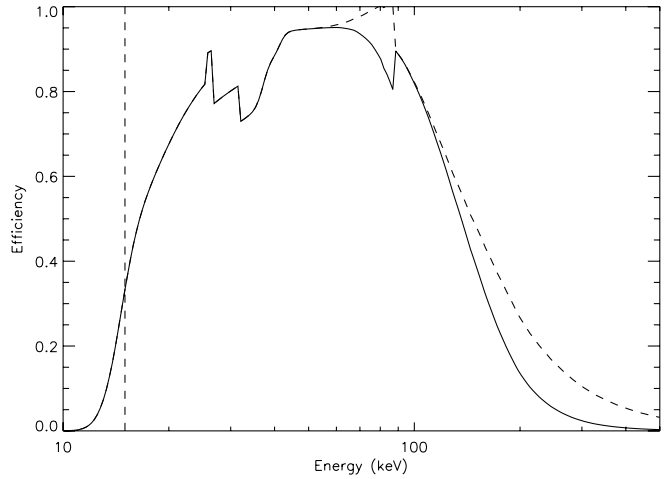

FIG. 2.—Detector efficiency of BAT. Both curves are calculated with the area of the detector plane divided by 2, accounting for the coded mask. Relevant for imaging, the net detector efficiency (*solid curve*) is the efficiency for the *difference* between the fluxes through the open and closed mask cells. The transparency of the closed mask cells at high energy reduces the source's coded signal. The gross detector efficiency (*dashed curve*) is the efficiency for the sum of the fluxes through the open and closed mask cells. In this case the mask transparency increases the number of source photons that reach the detector plane, increasing the gross efficiency.

Ideally, the closed cells of the mask (consisting of lead tiles) would be perfectly opaque, but at high energy (above $\sim$100 keV) the optical depth through the lead tiles decreases. Imaging with a coded mask relies on the shadow cast by the closed mask cells. However, if flux leaks through the closed mask cells, then the contrast between the detector pixels that are illuminated by the source and those that are shadowed is reduced; this leakage is equivalent to no flux leaking through the closed mask cells and the detection of less flux by the illuminated detector pixels. The solid curve in Figure 2 is the net detector efficiency, the efficiency for the difference between the fluxes through the open and closed mask elements, which is relevant for imaging. Because the imaging step is the most restrictive part of BAT's trigger, the net detector efficiency is used to calculate the source counts for the sensitivity.

The dashed curve in Figure 2 is the gross detector efficiency, the efficiency for the sum of the fluxes through the open and closed mask elements. The product of the gross detector efficiency, the incident flux, the total detector area, and the fraction of the coded mask that is open (half for BAT) results in the total count rate. The gross detector efficiency is relevant for BAT's rate trigger.

Thus, the net detector efficiency is reduced at the energies where the mask's lead tiles are partially transparent, while the gross detector efficiency is increased at the same energies because more source photons reach the detector plane. Note that the rate trigger and imaging use different detector efficiencies and will have somewhat different energy dependencies.

CZT has high quantum efficiency below 100 keV. However, the optical depth through the mask substrate that supports both the closed and open mask cells results in the roll-off in the detector efficiency at low energy ($<$40 keV). This low-energy roll-off reduces the aperture flux (i.e., the cosmic X-ray background), which dominates the total background at low energy, but also decreases BAT's sensitivity to X-ray flashes and X-ray-rich bursts.

BAT's total on-orbit background rate is approximately $\sim$10 kHz, consistent with prelaunch estimates. At low energies the background is dominated by the aperture flux (the cosmic X-ray background through the mask), while at high energy instrumental background and aperture flux through BAT's side shields (which become transparent at $\sim$100 keV) increase the background. The background varies over an orbit, and I use the lowest observed background rates in the energy bands used by BAT's burst trigger: $\sim$2300 Hz for $\Delta E = 15$–25 keV, $\sim$4700 Hz for $\Delta E = 15$–50 keV, $\sim$4700 Hz for $\Delta E = 25$–100 keV, and $\sim$4700 Hz for $\Delta E = 50$–500 keV. The background is near this minimum about half the time; the reduction in sensitivity resulting from higher backgrounds reduces the overall burst detection rate by about 5%. Note that for $B = 4700$ counts in 1 s, $C_s \sim S_{i,\mathrm{th}}\sqrt{B}/f_m \sim 700$, and thus $C_s \ll B$ at a threshold value of $S_{i,\mathrm{th}} = 7$; the assumption that the background dominates is valid.

I parameterize the spectrum with the Band function (Band et al. 1993), which is a smoothly broken power law with low-energy spectral index α [$N(E) \propto E^{\alpha}$] and high-energy spectral index β [$N(E) \propto E^{\beta}$]. The characteristic energy is the peak energy E_p, the photon energy of the peak of the $E^2N(E) \propto \nu f_\nu$ spectrum. The spectrum can be normalized by the flux integrated over a specified energy band, which need not be the same as ΔE. I use F_T, the peak flux in the 1–1000 keV band.

Figure 3 compares the maximum sensitivity for BATSE (*left*) and BAT on-axis (*right*) for $\Delta t = 1.024$ s. The sensitivity is the threshold peak photon flux F_T at which the detector triggers.

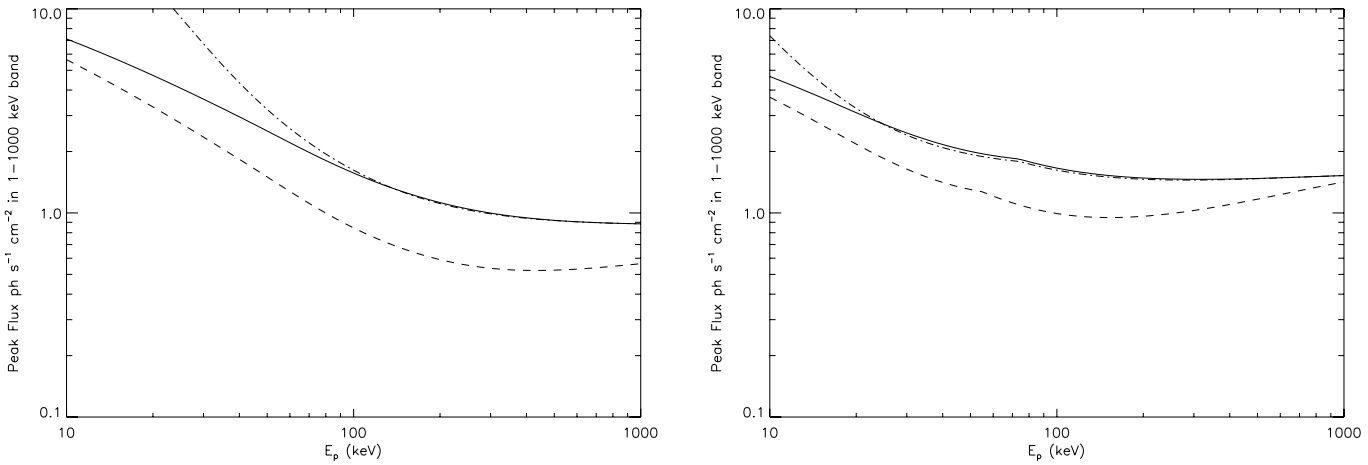

FIG. 3.—Maximum detection sensitivity for BATSE's LAD (*left*) and *Swift*'s BAT (*right*) for $\Delta t = 1.024$ s. *Solid line*: $\alpha = -1$, $\beta = -2$; *dashed line*: $\alpha = -0.5$, $\beta = -2$; *dot-dashed line*: $\alpha = -1$, $\beta = -3$.

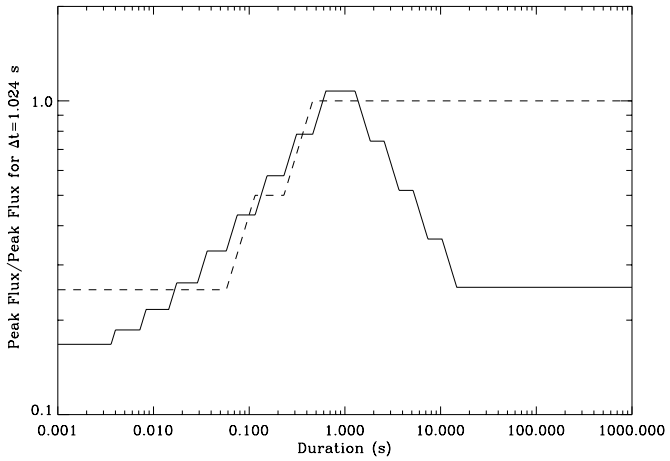

FIG. 4*a*

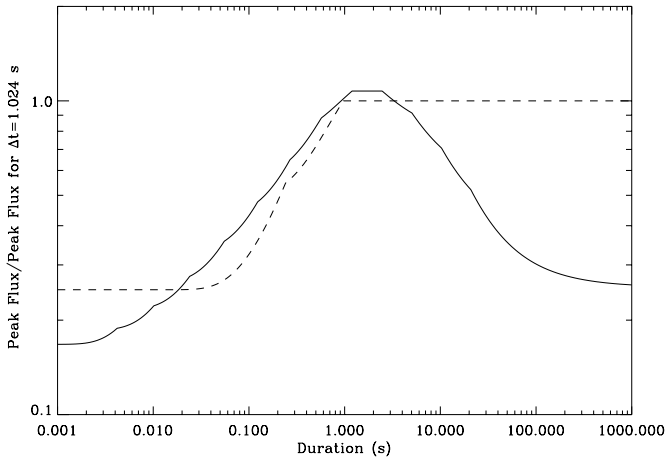

FIG. 4*b*

FIG. 4.—Ratio of the threshold peak flux for a detector's set of accumulation times Δt to the peak flux for $\Delta t = 1.024$ s as a function of the burst duration T_{90}. The solid curve shows the ratio for BAT resulting from requiring the detection of a statistically significant source in an image. The dashed curve is the ratio for BATSE's set of Δt. (*a*) A flat-top burst light curve; (*b*) an exponential light curve.

Because the threshold is expressed in the same units—the flux in the 1–1000 keV band—regardless of ΔE, the sensitivity of different detectors, and of different ΔE for the same detector, can be compared (Band 2003). These thresholds depend on the burst's spectral parameters, which determine the shape of the spectrum (not its normalization). The curves on Figure 3 show the threshold flux as a function of E_p, holding the low- and high-energy spectral indices α and β fixed. BAT runs its trigger on four different ΔE simultaneously ($\Delta E = 15$–25, 15–50, 25–100, and 50–500 keV), and the detector sensitivity is the lowest threshold at any given E_p, resulting in the scalloping of the BAT sensitivity curves.

As can be seen, on-axis BAT is less sensitive than BATSE's maximum sensitivity for $E_p > 100$ keV by a factor of $\sim$1.5, and is more sensitive at lower E_p values, again by a factor of $\sim$1.5, for the same $\Delta t = 1.024$ s. As discussed below, BAT's overall sensitivity depends on both its sensitivity at fixed Δt and the sensitivity resulting from triggering on multiple values of Δt.

2.3. *Duration Dependence*

I now consider BAT's sensitivity to bursts with different durations. BATSE used a rate trigger with three values of Δt (0.064, 0.256, and 1.024 s), while after a rate trigger BAT can form images on a variety of timescales ranging from 0.004 to 26 s. In addition, BAT forms images every 64 and 320 s without a rate trigger.

The relationship between burst duration and the detector accumulation time Δt is illustrated by considering a constant-flux burst of duration T when the background dominates the source. If $T > \Delta t$, that is, if the flux remains constant over Δt, then the threshold flux is proportional to $\Delta t^{-1/2}$ (i.e., fainter bursts will be detected as Δt increases): the number of source counts increases as Δt, but the square root of the background increases only as $\Delta t^{1/2}$. However, when $T < \Delta t$ (the light curve is a short spike relative to the accumulation time), then the threshold flux is proportional to $\Delta t^{1/2}$ (i.e., bursts must be brighter to be detected for longer Δt): the number of source counts remains constant, but the square root of the background increases as $\Delta t^{1/2}$.

Imaging is the final, determining step of BAT's trigger, and for short Δt the background may not dominate the source counts C_s in the denominator of equation (2); the addition of C_s to B increases the denominator and therefore decreases S_i relative to a simple rate trigger (eq. [1]). Assume that the light curve is $PAh(t; T_{90})$, where P is the instantaneous peak flux accumulated over ΔE, and A is the detector area. With a maximum value of 1, the light curve function $h(t; T_{90})$ parameterizes the light curve in terms of duration T_{90}. The number of burst counts accumulated in Δt_i is therefore $C_s = \int_0^{\Delta t_i} PAh(t; T_{90})dt$, where I assume that $h(t; T_{90})$ peaks within Δt and I ignore the issue of the registration of the burst relative to the time bin boundaries (i.e., I assume that Δt begins at the beginning of the burst, and ignore the possibility that the fluent part of the burst light curve straddles two time bins). Next, let b be the background rate in ΔE for the entire detector; thus, the number of background counts is $B = b\Delta t$. For my calculations I use $b = 4700$ counts s^{-1}.

For a given T_{90} and Δt I calculate the threshold value for a rate trigger $P_{\mathrm{th},r}(T_{90}; \Delta t)$ assuming a threshold value of S_r in equation (1) and for an image trigger $P_{\mathrm{th},i}(T_{90}; \Delta t)$ assuming a threshold value of S_i in equation (2). Note that S_r is applicable to BATSE's rate trigger, but not to BAT's. When there are multiple accumulation times $\{\Delta t_i\}$, then the resulting threshold peak flux P_{th} is the minimum P_{th} for the different Δt_i values at a given T_{90}. Since BATSE established a very large, statistically homogeneous burst database for $\Delta t = 1.024$ s, and many burst distributions are normalized for this value of Δt, I normalize P_{th} for different Δt values and trigger types to the $P_{\mathrm{th},r}$ for a rate trigger with $\Delta t = 1.024$ s.

Figure 4*a* uses $h(t; T_{90}) = 1$ over the duration of the burst, while Figure 4*b* uses $h(t) = \exp(-t/\tau)$, where $T_{90} = \tau \ln 10$. On both figures the ratio $P_{\mathrm{th}}(T_{90}; \{\Delta t_i\})/P_{\mathrm{th},r}(T_{90}; \Delta t = 1.024\ \mathrm{s})$ is plotted as a function of T_{90} for rate or image triggers and different sets of Δt. The dashed curve is for a rate trigger with BATSE's three values of $\Delta t = 0.064$, 0.256, and 1.024 s; the plotted ratio is $P_{\mathrm{th},r}(T_{90}; \{\Delta t_i\}_{\mathrm{BATSE}})/P_{\mathrm{th},r}(T_{90}; \Delta t = 1.024\ \mathrm{s})$. The decrease for durations T_{90} less than $\sim$1 s shows the increase in sensitivity to short duration bursts that resulted from BATSE adding $\Delta t = 0.064$ and 0.256 s to $\Delta t = 1.024$ s. The solid curve shows the ratio $P_{\mathrm{th},i}(T_{90}; \{\Delta t_i\}_{\mathrm{BAT}})/P_{\mathrm{th},r}(T_{90}; \Delta t = 1.024\ \mathrm{s})$ for the BAT image trigger with Δt ranging from 0.004 to 26 s. As can be seen, adding Δt values both greater than and less than BATSE's set increases the sensitivity to both longer and shorter duration bursts. The increase in sensitivity for short-duration bursts is not very great, because $C_s \sim B$ (see the denominator of eq. [2]); this is an unavoidable feature of the imaging required to localize bursts.

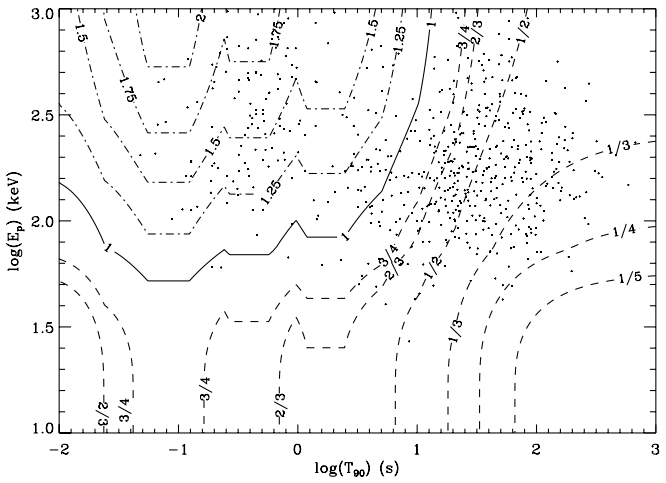

FIG. 5*a*

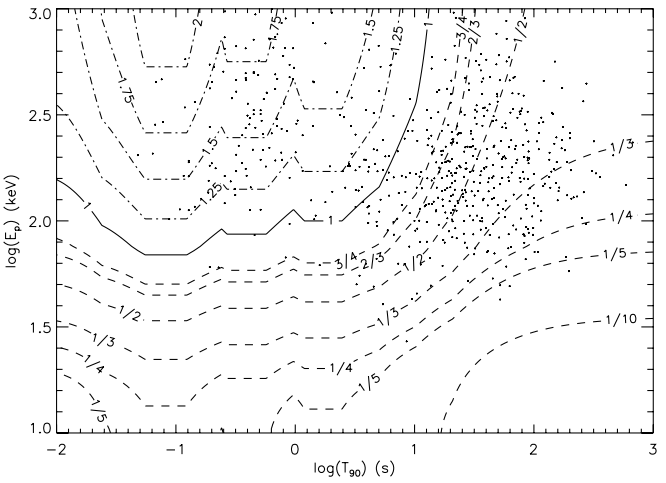

FIG. 5*b*

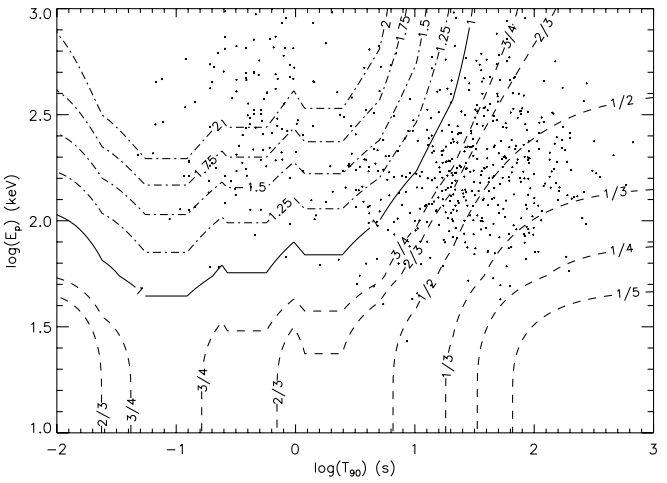

FIG. 5*c*

FIG. 5.—Contour plot of the ratio of the sensitivities of BAT and BATSE as a function of E_p and T_{90}; a ratio less than 1 indicates that BAT is more sensitive than BATSE at that particular set of E_p and T_{90}. Also plotted are the E_p and T_{90} for a set of BATSE bursts with enough counts for spectral fits. The energy and temporal effects were treated separately; differences in the burst light curve in different energy bands were not considered. (*a*) $\alpha = -1$ and $\beta = -2$; (*b*) $\alpha = -1$ and $\beta = -3$; (*c*) $\alpha = -0.5$ and $\beta = -3$.

Because burst light curves have very different shapes, calculating a general detector sensitivity as a function of T_{90} is very difficult. For example, Figures 4*a* and 4*b* show that the increase in sensitivity for long-duration bursts occurs at longer durations for the exponential light curves than for flat-top light curves. Applying the BAT trigger code to an ensemble of typical observed burst light curves (e.g., from BATSE) would provide a better estimate of the sensitivity as a function of duration (see Fenimore et al. 2004).

In summary, the longer Δt_i values significantly increase BAT's sensitivity to long-duration bursts. BAT's increase in sensitivity to short bursts relative to BATSE is not as great, because the number of source counts becomes comparable to the number of background counts.

3. RESULTING OBSERVED BURST POPULATION

BAT detects mostly long-duration bursts, as shown by Figure 1 (although the few short bursts have been very revealing). On average, long-duration bursts are softer than short-duration bursts (Kouveliotou et al. 1993). BAT's detector efficiency shifts its sensitivity to lower energies than BATSE's (Berger et al. [2005] noted this factor), and its use of longer Δt values increases its sensitivity to long-duration bursts. In addition, most bursts show significant hard-to-soft spectral evolution (Ford et al. 1995), and therefore their low-energy emission lasts longer; this is an effect not considered by studying the spectral and temporal dependencies separately. Consequently, a longer accumulation time increases the effectiveness of a lower energy trigger band for long-duration bursts.

While BAT's array of accumulation times increases its sensitivity to both very short and long-duration bursts relative to BATSE's set of $\Delta t = 0.064$, 0.256, and 1.024 s, the increase in sensitivity is much greater for long bursts than for short bursts. Whether BATSE's trigger truncated the duration distribution on the short side has been debated (e.g., Lee & Petrosian 1996); unfortunately, BAT's relatively small increase in short-duration sensitivity (and its lower energy band) make it difficult to determine whether a large population of short-duration bursts exists. An analysis of short-duration rate triggers that do not result in successful image triggers might address this issue.

Combining the results of § 2.2 and § 2.3, Figures 5*a*, 5*b*, and 5*c* show the ratio of BAT to BATSE flux thresholds as a function

of duration T_{90} and peak energy E_p for three different sets of spectral indices. These figures treat the energy and temporal factors independently. Ratio values less than 1 indicate that BAT is more sensitive than BATSE. Also shown are a sample of BATSE bursts for which values of T_{90} and E_p are available (Mallozzi et al. 1998); the bursts in this sample provided enough counts for spectral fits. As can be seen, the short, hard bursts are in a region of parameter space where BAT is less sensitive than BATSE, while BAT is more sensitive to long, soft bursts. The gradient of the contours shows that BAT detects fewer short, hard burst because its energy band is lower than BATSE's was, and BAT detects more long, soft bursts because of both its lower energy band and its greater sensitivity to long bursts. This is consistent with the shift in the duration distributions in Figure 1. BAT's greater sensitivity to long-duration bursts is consistent with the average fluence of the *Swift* bursts being a factor of $\sim$2.5 fainter than the average fluence of the BATSE bursts (T. Sakamoto 2005, private communication).

When a burst occurs at high redshift, its observed spectrum is redshifted (i.e., becomes softer) and its observed duration is dilated. Thus, the burst is shifted toward the parameter space region in which BAT's sensitivity increase is greatest. However, evolution of the average burst's intrinsic spectrum and duration obviously determines where the burst began, and therefore ends, in parameter space.

BeppoSAX and *HETE-II* also detect(ed) and localize(d) bursts by forming images in low-energy bands with accumulation times longer than 1 s, and the bursts detected by both detectors are almost exclusively long-duration bursts. *BeppoSAX* formed images in the 1.8–28 keV band, and *HETE-II* forms images in the 2–25 keV band (*HETE-II* also forms images in a softer band). Thus, the same factors that favor the detection of long bursts in BAT's burst sample are relevant to these two detectors.

The burst detection rate depends on the spectral and temporal sensitivities discussed in § 2.2 and § 2.3, respectively, and the FOV. BAT's sensitivity decreases off-axis, first as a result of area foreshortening (i.e., the detector plane is not perpendicular to the direction to an off-axis source) and then because the outer regions of the FOV are only partially coded. In the partially coded region, the source flux falls on only part of the detector plane, but the entire detector plane contributes background counts. To reduce the dilution of source counts by background from sections of the detector plane that are not illuminated by a source in the partially coded region of the sky, the BAT detector plane is broken into quadrants; each of the four quadrants, all four pairs of adjoining quadrants, and the entire detector plane are treated as independent detectors simultaneously. Thus, the burst detection sensitivity varies across the FOV, and fainter bursts will be detected near the center of the FOV, while only bright bursts will be detected near the edges. Using BATSE's burst rate as a function of peak flux (Band 2002) and BAT's sensitivity across its FOV, compensating for BAT's different energy and temporal dependencies, and accounting for various operational factors (e.g., the dead time resulting from slews and South Atlantic Anomaly passages) results in an estimated burst detection rate that is consistent with the observed detection rate of $\sim$100 bursts per year.

4. SUMMARY

Swift's burst sensitivity depends on the imaging performance of BAT, *Swift*'s coded mask gamma-ray detector. Using a simplified model of BAT's trigger, my analysis focused on the sensitivity to bursts' temporal and spectral properties separately. Because of the large burst database it has accumulated, BATSE is the reference detector to which I compare BAT.

As expected from the detectors' detecting material (BAT's CZT vs. BATSE's NaI [Tl]), BAT's energy band is shifted to lower energies than BATSE's was. Thus, for same accumulation time (e.g., $\Delta t = 1.024$ s), BAT is less sensitive than BATSE for $E_p > 100$ keV but more sensitive for lower E_p. Note that the relative sensitivity at fixed Δt is only one component of the comparison between detectors.

The BAT forms images by accumulating counts on timescales much longer (up to 26 s) than BATSE's rate trigger (up to 1.024 s), increasing BAT's sensitivity to long-duration bursts. Because the number of burst counts is comparable to the number of background counts for short bursts, BAT's image trigger is not as sensitive to short bursts as a simple rate trigger would be; however, a rate trigger would not localize the bursts. A study of statistically significant rate triggers of short bursts that did not result in statistically significant point sources might determine whether there is a large population of as yet undetected short bursts.

The longer accumulation times increase BAT's sensitivity to long-duration bursts, particularly for bursts with a high level of emission over an extended period (as opposed to long-duration bursts dominated by a short spike). The BAT detects bursts in a lower energy band than BATSE did, and long-duration bursts are softer, on average, than short-duration bursts. Consequently, BAT preferentially detects long-duration bursts. Spectral redshifting and time dilation of a burst's duration move high-redshift bursts into the parameter region where BAT is more sensitive. The same trigger characteristics explain why *BeppoSAX* and *HETE-II* also detect(ed) long-duration bursts.

I emphasize that my semianalytic calculations use a simplified model of the complex BAT trigger system and my goal is to determine how BAT's hardware and trigger shape the burst population BAT detects. My goal is *not* to develop an accurate description of the detection threshold, which is very difficult if not impossible given the complex trigger and the time-varying background.

I thank S. Barthelmy, E. Fenimore, N. Gehrels, D. Hullinger, H. Krimm, D. Palmer, A. Parsons, T. Sakamoto, G. Skinner, and J. Tueller for their assistance and advice, and for the preliminary data about BAT they made available.

REFERENCES

Band, D. 2002, ApJ, 578, 806
———. 2003, ApJ, 588, 945
Band, D., et al. 1993, ApJ, 413, 281
Barthelmy, S., et al. 2005, Space Sci Rev, 120, 143
Berger, E., et al. 2005, ApJ, 634, 501
Burrows, D., et al. 2005, Space Sci Rev, 120, 165
Fenimore, E. E., Palmer, D., Galassi, M., Tavenner, T., Barthelmy, S., Gehrels, N., Parsons, A., & Tueller, J. 2003, in AIP Conf. Proc. 662, Gamma-Ray Burst and Afterglow Astronomy 2001, ed. G. Ricker & R. Vanderspek (Woodbury: AIP), 491
Fenimore, E. E., et al. 2004, Baltic Astron., 13, 301
Ford, L. A., et al. 1995, ApJ, 439, 307

Gehrels, N., et al. 2004, ApJ, 611, 1005
Grindlay, J. 2005, NewA Rev., 49, 436
Kouveliotou, C., Meegan, C. A., Fishman, G. J., Bhat, N. P., Briggs, M. S., Koshut, T. M., Paciesas, W. S., & Pendleton, G. N. 1993, ApJ, 413, L101
Lee, T., & Petrosian, V. 1996, ApJ, 470, 479
Mallozzi, R., et al. 1998, in AIP Conf. Proc. 428, 4th Huntsville Symposium on Gamma-Ray Bursts, ed. C. Meegan, R. Preece, & T. Koshut (Woodbury: AIP), 273
McLean, K., Fenimore, E. E., Palmer, D., Barthelmy, S., Gehrels, N., Krimm, H., Markwardt, C., & Parsons, A. 2004, in AIP Conf. Proc. 727, Gamma-Ray Bursts: 30 Years of Discovery, ed. E. E. Fenimore & M. Galassi (Melville: AIP), 667
Osborne, J., et al. 2005, Proc. SPIE, 5898, 352
Palmer, D. M., et al. 2004, in AIP Conf. Proc. 727, Gamma-Ray Bursts: 30 Years of Discovery, ed. E. E. Fenimore & M. Galassi (Melville: AIP), 663
Roming, P., et al. 2005, Space Sci. Rev., 120, 95